Open-Circuit Voltage Deficit, Radiative Sub-Bandgap States, and Prospects in Quantum Dot Solar Cells

Chia-Hao Marcus Chuang[†], **Andrea Maurano**[‡], **Riley E. Brandt**[§], **Gyu Weon Hwang**[†], **Joel Jean**[‡], **Tonio Buonassisi**[§], **Vladimir Bulovi**[‡], and **Moungi G. Bawendi**[*,‖]

[†]Department of Materials Science and Engineering, Cambridge, Massachusetts 02139, United States

[‡]Department of Electrical Engineering and Computer Science, Cambridge, Massachusetts 02139, United States

[§]Department of Mechanical Engineering, Massachusetts 02139, United States

[‖]Department of Chemistry, Massachusetts Institute of Technology, Cambridge, Massachusetts 02139, United States

Abstract

Quantum dot photovoltaics (QDPV) offer the potential for low-cost solar cells. To develop strategies for continued improvement in QDPVs, a better understanding of the factors that limit their performance is essential. Here, we study carrier recombination processes that limit the power conversion efficiency of PbS QDPVs. We demonstrate the presence of radiative sub-bandgap states and sub-bandgap state filling in operating devices by using photoluminescence (PL) and electroluminescence (EL) spectroscopy. These sub-bandgap states are most likely the origin of the high open-circuit-voltage (V_{OC}) deficit and relatively limited carrier collection that have thus far been observed in QDPVs. Combining these results with our perspectives on recent progress in QDPV, we conclude that eliminating sub-bandgap states in PbS QD films has the potential to show a greater gain than may be attainable by optimization of interfaces between QDs and other materials. We suggest possible future directions that could guide the design of high-performance QDPVs.
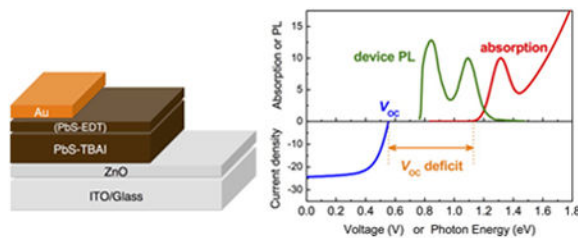
[*]Corresponding Author: mgb@mit.edu.

Notes: The authors declare no competing financial interest.

Keywords

quantum dot; PbS; sub-bandgap state; photovoltaics; solar energy

Developing low-cost technologies for efficient solar energy harvesting has long been a goal of energy sustainability. In the past decade, solution-processed solar cells based on lead chalcogenide (PbX, X = S, Se, Te) colloidal quantum dots (QDs) have become one emerging photovoltaic (PV) technology[1] that can potentially meet this goal. Bulk lead chalcogenides have bandgaps below 0.5 eV. Owing to the quantum confinement effect, the bandgap of lead chalcogenide QDs can be tuned from approximately 0.6 to 1.5 eV. The unique combination of a low bandgap energy and broad tunability enables infrared photon harvesting and the development of multijunction solar cells.[2] Among lead chalcogenide QDs, PbS has received the most attention for solar cell applications. Their inexpensive and Earth-abundant nature,[3] scalable synthesis, good stability, and solution-processability make PbS QDs a promising candidate for low-cost solar cells. Indeed, the certified QDPV efficiency record has rapidly increased from 3% to >9% within 4 years, predominantly due to improvements in PbS QDPV.[1,4–8] The feasibility of PbS QDPV on flexible plastic substrates has been successfully demonstrated.[9] Device stability has also rapidly improved, with reports of >1000 h of operation stability[4,10] and >150 days of air stability.[8]

Despite recent advances, the power conversion efficiency of QDPV is still below the expected performance for a semiconductor with this bandgap range. One primary limitation is the large open-circuit voltage (V_{OC}) deficit (defined as $E_g/q - V_{OC}$, where E_g is the absorber bandgap and q is the elementary charge). This large V_{OC} deficit is often seen in QDPVs regardless of device structure and surface ligands, but its origin is not fully understood. Recently, halide-based ligands (i.e., Cl^-, Br^-, I^-) have been shown to improve the stability of PbS and PbSe QDs.[8,11–15] Although QDPVs made of halide-passivated QDs achieve high short-circuit current densities (J_{SC}) and efficiencies, they typically exhibit somewhat lower V_{OC} values than devices employing organic ligand-passivated QDs.[6–8,16] This phenomenon cannot be explained in terms of the degree of surface passivation and is not fully understood. In this work, we investigate the working mechanism of efficient PbS QD solar cells. We identify the possible origins of the large V_{OC} deficit. In particular, we show evidence for the presence of radiative sub-bandgap states, based on photoluminescence (PL) and electroluminescence (EL) measurements on operating photovoltaic devices. These states likely account for both the V_{OC} deficit and the limited carrier collection. On the basis of these findings, future prospects for QDPV are discussed, and potential routes to improving QDPV performance are suggested.

The devices investigated in this work are planar hetero-junction ZnO/PbS QD solar cells with an iodide-passivated PbS QD absorber layer. This layer is formed by solid-state ligand exchange with tetrabutylammonium iodide (TBAI). For some devices, a thin layer of 1,2-ethanedithiol(EDT)-passivated PbS QDs is introduced as an electron-blocking layer between the PbS-TBAI QD layer and Au electrode (Figure 1a). This PbS-TBAI QD/PbS-EDT QD device structure yields some of the highest efficiency QD solar cells to date. Experimental details are provided in the Supporting Information and in our previous publication.[8]

As shown in Figure 1b, the qV_{OC} (555 meV) of a certified 8.6% device[8] is significantly lower than the absorption onset energy of a PbS-TBAI QD film. Figure 1c and d compare the V_{OC} deficit in QDPV with that of other leading PV technologies, with V_{OC} values corresponding to certified record-efficiency devices.[17] As the definition of bandgap differs between communities, we consider a range between two values for the PbS QD bandgap: the optical gap, conventionally defined as the first exciton absorption peak (here, 1.33 eV), and the onset of the external quantum efficiency (EQE) (1.13 eV). Given the broad exciton absorption peak in QDs, the EQE onset is preferred when comparing the measured V_{OC} with the Shockley–Queisser limit.[18] Although the V_{OC} deficit (575 mV) in QDPV is comparable to that in CdTe and CZTSSe solar cells, it is ~200 mV larger than that in single-crystalline Si solar cell with a similar bandgap (E_g = 1.12 eV, V_{OC} = 740 mV).

Sources of V_{OC} deficit could be (1) poor QD monodispersity,[19] (2) insufficient photon absorption, (3) incomplete charge collection, and (4) fast carrier recombination rate. Poor monodispersity of QDs broadens the absorption spectrum near the band-edge, whose sharpness is known to be correlated with device V_{OC}.[19,20] However, monodispersity is unlikely to be the primary cause of the large V_{OC} deficit, as has been shown previously[11,21,22] and discussed in the Supporting Information. Insufficient absorption and incomplete charge collection are also not likely primary causes of the large V_{OC} deficit as V_{OC} scales logarithmically with J_{SC}. Thus, we focus our attention on carrier recombination mechanisms, which are dominated by junction characteristics and the presence of sub-bandgap states in the absorber (i.e., the sub-bandgap emissive states in Figure 1b).

We carried out several device characterization techniques to investigate the working mechanisms of these devices. The diode ideality factor n is an indicator of the dominant recombination mechanism. By fitting the dark J–V curves with the ideal diode equation, n is determined to be 1.8 ± 0.1 for both PbS-TBAI QD and PbS-TBAI QD/PbS-EDT QD devices (Figure 2a). Alternatively, n is found to be 1.5 ± 0.1 from the light intensity dependence of the short-circuit current density (J_{SC}) (Figure 2b) and V_{OC} (Figure 2c) according to the following relation:

$$V_{OC} = \frac{nkt}{q} \ln \left(\frac{J_{SC}}{J_0} \right) \quad (1)$$

where k is the Boltzmann constant, T the temperature, and J_0 the reverse saturation current density. When band-to-band recombination dominates, n is equal to 1. The ideality factor n > 1 indicates that other recombination mechanisms such as trap-assisted recombination (n = 2) in PbS QDs within the space-charge region (or depletion region) are involved.

The similarity in the ideality factor and dark J–V characteristics of the PbS-TBAI QD and PbS-TBAI QD/PbS-EDT QD devices suggest similar recombination mechanisms, which points to two important conclusions. First, the higher V_{OC} of the PbS-TBAI QD/PbS-EDT QD device compared to the PbS-TBAI QD device is a consequence of its higher J_{SC} under the same light intensity. This is consistent with the electron-blocking effect of the PbS-EDT QD layer, which improves the charge carrier collection efficiency.[8] Second, since the addition of the PbS-TBAI QD/PbS-EDT QD interface does not appear to affect carrier

generation-recombination mechanisms, the ZnO/PbS QD heterojunction must dominate the carrier recombination processes (J_0) and thus the V_{OC}. The dominant recombination process is, thus, either space-charge region recombination in PbS-TBAI QDs or interfacial recombination at the ZnO/PbS-TBAI QD interface.

Figure 2d shows a study of carrier recombination dynamics using transient photovoltage measurements at various steady-state bias light intensities. The carrier lifetimes as a function of V_{OC} for PbS-TBAI QD and PbS-TBAI QD/PbS-EDT QD devices are almost identical, further supporting similar dominant recombination mechanisms and rate constants. Zhao et al.[23] and Brown et al.[24] have shown that different PbS QD layers can alter both the carrier lifetimes and their slopes versus V_{OC}. When different recombination mechanisms are present, a longer carrier lifetime usually translates into a higher V_{OC}. In contrast, the devices studied here have identical ZnO/PbS QD heterojunctions. Under identical white light bias, the PbS-TBAI QD/PbS-EDT QD device—which exhibits a higher V_{OC}—shows a shorter carrier lifetime, due to the higher steady-state photogenerated carrier concentration. We note that under 1 sun illumination (100 mW/cm^2), the carrier lifetimes for PbS-TBAI QD/PbS-EDT QD and PbS-TBAI QD devices are 0.8 and 1.4 μs, respectively, which indicates faster recombination rates than observed in devices based on PbS-EDT QDs (2 μs, Supporting Information Figure S2) and other organic ligand-passivated PbS QDs (2–13 μs).[24,25]

The temperature-dependent J–V characteristics provide further insight into generation-recombination processes contributing to the diode current (Figure 3a-c). For a single thermally activated carrier generation-recombination mechanism, J_0 can be expressed as eq 2. Substitution of eq 2 into eq 1 yields eq 3

$$J_0 = J_{00}\exp\left(\frac{-E_a}{nkt}\right) \quad (2)$$

$$V_{OC} = \frac{E_a}{q} - \frac{nkT}{q}\ln\left(\frac{J_{00}}{J_{SC}}\right) \quad (3)$$

where E_a is the activation energy, and J_{00} the prefactor.[26] n activation energy equal to the absorber bandgap implies the dominance of bulk generation-recombination in the absorber. An activation energy smaller than the bandgap often implies the significance of interfacial recombination.[26] In the high-temperature range where n, J_{00}, and J_{SC} are nearly temperature-independent, E_a can be determined by extrapolating V_{OC} to 0 K. As shown in Figure 3a, for a PbS-TBAI QD/PbS-EDT QD device, E_a is determined to be 0.92 ± 0.01 eV for all three illumination intensities. In the range where n, J_{00}, and J_{SC} show temperature dependence, E_a can be determined from eq 4, a reorganized form of eq 2[26]

$$n\ln(J_0) = -\frac{E_a}{kT} + n\ln(J_{00}) \quad (4)$$

From eq 4 and the dark J–V curves at different temperatures (Figure 3b), E_a is determined to be 0.94 ± 0.01 eV (Figure 3d), in good agreement with the value extracted from the T–V_{OC}

plot (Figure 3a). The PbS-TBAI QD device shows similar behavior with an activation energy of 0.96 ± 0.01 eV.

Figure 4a shows the PL spectra of a PbS-TBAI QD/PbS-EDT QD device under different excitation intensities. An additional emission peak with energy ∼0.23 eV lower than the band-edge emission is observed. This sub-bandgap emission dominates the PL at low excitation intensities. sub-bandgap emission is also observed in PbS-TBAI QD films on glass that are fabricated and encapsulated in an air-free environment (Supporting Information Figure S6a), which suggests that it originates neither from interfacial states between ZnO and PbS-TBAI QDs nor from any oxidation species in PbS-TBAI QDs. The excitation power dependence (Figure 4b) is consistent with a competition between two emissive species, where the free-exciton-like transitions exhibit superlinear power dependence with an exponent $1 < a < 2$, whereas transitions involving states within the gap follow a sublinear power dependence ($a < 1$).[27] The fact that the sub-bandgap emission has not saturated suggests that these sub-bandgap states may not be completely filled at 1 sun intensity.

The device also shows electroluminescence (EL) with a turn-on voltage of approximately 0.5 V (Figure 4c). The ratio of the sub-bandgap emission to the band-edge emission in the EL spectra decreases with increasing applied voltage (i.e., with increasing injected carriers density (Supporting Information Figure S5), similar to the power-dependent PL spectra. Unlike the band-edge emission whose peak position stays constant, the sub-bandgap emission shows a blue shift with increasing excitation power (PL) (Figure 4a) or injected carriers (EL) (Supporting Information Figure S5), consistent with filling of sub-bandgap states from deeper states in PbS QDs.

Additional information can be found in the emission spectra at different applied biases (Figure 4d). As the applied voltage increases from reverse to forward bias, the PL intensity increases (Figure 4e), whereas the extracted photocurrent decreases monotonically (Supporting Information Figure S4). This observation is similar to that in a recent study[28] and indicates that uncollected photogenerated carriers in part contribute to the PL in a working device. Moreover, at higher forward bias, the ratio of sub-bandgap PL to band-edge PL decreases, and the sub-bandgap PL slightly blue-shifts (Figure 4f). Such behavior is consistent with sub-bandgap state filling.

On the basis of the experimental results described above, we discuss the origins of the V_{OC} deficit. One component of the V_{OC} deficit is the below-bandgap activation energy ($E_a \sim$ 0.92 eV) for dark current generation, which can be interpreted in two scenarios: (1) Interfacial recombination could be a dominant process, and E_a represents the bandgap of PbS QDs minus the conduction band offset between ZnO and PbS QDs. (2) E_a is the energy difference between the sub-bandgap states and the band edge—the "effective gap" in QDs. As we discuss below, scenario 2 appears more likely to be the origin of the below-bandgap activation energy.

If interfacial recombination at the ZnO/PbS QD heterojunction is the dominant mechanism (scenario 1), optimization of the ZnO/PbS QD interface by tuning the band-edge energy

levels or carrier concentration of ZnO could potentially improve the V_{OC}. Enhancement of V_{OC} via these approaches has been seen,[25,29–31] yet the observed V_{OC} values are similar to those reported elsewhere and remain considerably lower than the bandgap. In addition, caveats exist in determining the band alignment at heterojunctions. In related literature, the band-edge positions of oxides and QDs are often measured individually and referenced to the vacuum level to form the band diagram. This approach could be inaccurate, as we discuss in the Supporting Information. In short, surface states, surface dipoles, gap states, and chemical interactions between two materials could affect the band offset or cause Fermi level pinning.[32] Such phenomena have been seen in many QDPV systems.[5,8,33–35] Consequently, for discussion on the effects of interfacial band alignment engineering on device performance, performing direct measurements of the relative band alignment from bilayer samples may be more valuable.

In the case of scenario 2, the effective gap E_a is determined by the position of the sub-bandgap energy levels. The good agreement of the energy difference between the bandgap and E_a ($E_g - E_a \approx 0.21$ eV), and the energy difference between the band-edge and sub-bandgap state emission (∼0.23 eV), is consistent with this scenario. This energy difference is similar to the trap activation energy (∼0.26 eV) for PbS QDs of this size.[36] This scenario also explains the limits of achievable V_{OC} from interface engineering of the oxide layer in previous reports.[25,29–31] In scenario 2, the generation-recombination is dominated by *bulk* generation-recombination in QDs through the sub-bandgap states. Thus, the "effective gap" E_a represents the upper bound of the achievable V_{OC}. A similar effective gap concept has been proposed by Nagpal and Klimov, who further proposed the existence of a weakly conducting "mid-gap band" formed by these states for charge transport.[37] We confirm that EDT-treated QDs show similar sub-bandgap emission (Supporting Information Figure S6c), suggesting sub-bandgap states are not unique to halide-treated QDs. Therefore, this component of the V_{OC} deficit exists in organic ligand-passivated QDs as well. In fact, a below-bandgap E_a in organic ligand-passivated QDs has also been reported.[38]

Another component of the V_{OC} deficit at room temperature depends on the junction characteristics which determine the J_{SC}, n, and J_{00} (and thus the slope in Figure 3a). The latter two factors are not independent of each other, both being governed by recombination–generation mechanisms, carrier concentration, carrier mobility, and carrier lifetimes in the two materials forming the junction. (A brief discussion on the validity of carrier type,[39] concentration,[40] and mobility is provided in the Supporting Information).

The difference in the V_{OC} of organic and halide-passivated QD devices may be attributed to this second component of the V_{OC} deficit. As mentioned earlier, devices based on PbS-TBAI QDs show faster carrier recombination rates than devices based on organic ligand-passivated PbS QDs. In line with the fast recombination rate, the J_0 of our PbS-TBAI QD and PbS-TBAI QD/PbS-EDT QD devices, $(1.1 \pm 0.2) \times 10^{-4}$ mA/cm^2, is several orders of magnitude higher than that of other organic ligand-passivated PbS QDPVs (10^{-7}–10^{-5} mA/cm^2).[24,34,41] We argue that the high J_0 in PbS-TBAI QD devices may be due to the low hole concentration. On the basis of measured band positions, the Fermi level is closer to the midgap in PbS-TBAI QD than in PbS-EDT QD, suggesting a lower hole concentration in the former.[8] In a typical *p–n* junction, decreasing the hole concentration of the *p*-type

material (the PbS QD layer in the ZnO/PbS QD heterojunction) increases both J_0 and the p-side depletion width. For PbS QD cells with short carrier diffusion lengths (<100 nm),[42] the majority of collected photocarriers is generated within the depletion region. Therefore, a longer depletion width can improve photocurrent collection efficiency and thus J_{SC}. Nevertheless, the higher J_0 would also cause a reduction in V_{OC}. This argument may explain the general trend observed in QDPVs: devices based on PbS-TBAI QDs or other halide-passivated PbS QDs exhibit a higher J_{SC} than organic ligand-passivated PbS QDs,[6–8] but a lower V_{OC} due to the high recombination rate and J_0.

The sub-bandgap states may also be responsible for inefficient carrier collection, a significant loss in QDPVs with a thicker absorber layer. To date, the highest $J_{SC,EQE}$ (J_{SC} calculated by integrating the product of EQE and the AM1.5 solar photon flux; we note parenthetically that this calculation appears to have been performed incorrectly in some publications as we discuss in the Supporting Information) in QDPV is 26–29 mA/cm^2 for devices with an EQE onset of ∼1 eV.[16,43] The highest reported and independently verified J_{SC} is 24.2 ± 0.7 mA/cm^2 for a device with an EQE onset of ∼1.13 eV.[8] These values are only 60% of their corresponding theoretical maxima. It can be seen from Figure 5a that a device with a thin PbS-TBAI QD absorber (220 nm thick) shows a high internal quantum efficiency (IQE) of 70–80%, consistent with reported high IQE in lead chalcogenide QDs.[43,44] Clearly, insufficient absorption of long-wavelength photons limits EQE in thin devices. However, thicker devices benefit from increased absorption of long-wavelength photons at the expense of carrier collection efficiency (Figure 5b and 5c), a consequence of short carrier diffusion lengths. We believe it is the presence of the sub-bandgap states instead of carrier mobility that limits the carrier diffusion length. Although the trapped carrier density in PbS QDs seems relatively low, only 10^{-4}–10^{-2} per QD,[45,46] the corresponding volumetric concentration (10^{15}–10^{17} cm^{-3}) is comparable to or higher than the concentration of photogenerated carriers. At such high concentrations, increasing carrier mobility does not improve the carrier diffusion length.[19,46]

Although the midgap states or a "mid-gap band" in PbS QDs has been proposed to explain the photoresponse upon sub-bandgap excitation,[37,47] the origin of these states is not well understood.[7,48] It is likely that these states stem from off-stoichiometry. Indeed, first-principles calculations have shown that off-stoichiometry can introduce new localized sub-bandgap states.[49,50]

We speculate that these states are mainly introduced during the solid-state ligand exchange process. We find that the sub-bandgap emission is significant in QD thin films after solid-state ligand exchange with some short ligands such as TBAI and EDT (Supporting Information Figure S6c). In systems with long interparticle distances, only band-edge emission is observed (Supporting Information Figure S6). Due to low absorption cross sections, sub-bandgap states can be difficult to distinguish from the background signal in absorption spectra. The emission, on the other hand, can be significant because carriers originating from multiple QDs can be funneled to these sub-bandgap states (especially in systems with short inter-particle distance). This phenomenon is often seen in bulk semiconductors such as ZnO, GaN, and CdS.

The presence of sub-bandgap states limits both V_{OC} and carrier collection. The latter limitation has been mitigated by employing nanostructured oxides to improve carrier collection efficiency.[16,51,52] However, the fundamental problem regarding the presence of sub-bandgap states remains yet to be solved. Rath et al.[38] have demonstrated a bulk-heterojunction device structure that can fill the sub-bandgap states in the dark by blending ZnO and PbS QDs. These devices exhibit an E_a equal to their absorber bandgap (1.05 eV), an ideality factor close to 1, and a high V_{OC} (0.7 V) close to the theoretical limit, although poor charge transport in that device structure limits photocurrent collection and efficiency. This demonstration also supports our claims that interfacial recombination may not be the dominant process. Therefore, it is clear that eliminating sub-bandgap states in PbS QD films is essential to improving QDPV. This could show a greater potential gain than may be attainable by further optimization of the QD/oxide interfaces. A recent study indicates that the number of trap states influences J_0 and, thus, the V_{OC} deficit in metal–semiconductor–metal devices, implying a potential gain in V_{OC} by reducing the density of trap states.[36] It is worth noting that even with significant sub-bandgap states, current QDPVs still achieve efficiencies as high as ∼9%. Eliminating sub-bandgap states can potentially increase the diffusion length by reducing recombination and trapping in these states, leading to simultaneous and significant improvements in V_{OC} and J_{SC}. These improvements may well lead to power conversion efficiencies above 15%.

We highlight tailoring QD stoichiometry as a promising route to achieving this goal. Stoichiometric control of QDs has been demonstrated in PbSe QD Schottky devices by thermally evaporating excess Pb or Se atoms onto the surface.[53] Finding effective methods to control the stoichiometry across the whole QD layer may pave the way for highly efficient QDPVs. Possible strategies include exploring new ligands in combination with postdeposition treatments. In particular, employing recently developed halide ligands[6,54,55] and tuning the carrier concentration and stoichiometry could be promising approaches.

In summary, we have presented various analyses that provide a deeper understanding of the device working mechanisms and the present limitations in PbS QD solar cells. Our PL and EL studies unambiguously demonstrate the presence of sub-bandgap state filling effects in efficient PbS QDPVs. We show that the V_{OC} deficit can be attributed to two components: The below-bandgap activation energy accounts for a ∼0.2 V loss in the maximum achievable V_{OC} and is most likely due to the energy level of the sub-bandgap states. Inefficient carrier collection and heterojunction characteristics such as the low hole concentration in halide-treated PbS QDs account for remaining losses. We conclude that eliminating the sub-bandgap states is essential to improving the performance of PbS QDPVs. We discuss possible origins of these states and suggest future directions that could guide the design of highly efficient QD solar cells.

Supplementary Material

Refer to Web version on PubMed Central for supplementary material.

Acknowledgments

References

1. Research Cell Efficiency Records, National Renewable Energy Laboratory http://www.nrel.gov/ncpv/images/efficiency_chart.jpg.

2. Wang X, Koleilat GI, Tang J, Liu H, Kramer IJ, Debnath R, Brzozowski L, Barkhouse DAR, Levina L, Hoogland S, Sargent EH. Nat Photonics. 2011; 5:480–484.

3. Wadia C, Alivisatos AP, Kammen DM. Environ Sci Technol. 2009; 43:2072–2077. [PubMed: 19368216]

4. Luther JM, Gao J, Lloyd MT, Semonin OE, Beard MC, Nozik AJ. Adv Mater. 2010; 22:3704–3707. [PubMed: 20533423]

5. Gao J, Perkins CL, Luther JM, Hanna MC, Chen H, Semonin OE, Nozik AJ, Ellingson RJ, Beard MC. Nano Lett. 2011; 11:3263–3266. [PubMed: 21688813]

6. Tang J, Kemp KW, Hoogland S, Jeong KS, Liu H, Levina L, Furukawa M, Wang X, Debnath R, Cha D, Chou KW, Fischer A, Amassian A, Asbury JB, Sargent EH. Nat Mater. 2011; 10:765–771. [PubMed: 21927006]

7. Ip AH, Thon SM, Hoogland S, Voznyy O, Zhitomirsky D, Debnath R, Levina L, Rollny LR, Carey GH, Fischer A, Kemp KW, Kramer IJ, Ning Z, Labelle AJ, Chou KW, Amassian A, Sargent EH. Nat Nanotechnol. 2012; 7:577–582. [PubMed: 22842552]

8. Chuang CHM, Brown PR, Bulovi V, Bawendi MG. Nat Mater. 2014; 13:796–801. [PubMed: 24859641]

9. Loiudice A, Rizzo A, Grancini G, Biasiucci M, Belviso MR, Corricelli M, Curri ML, Striccoli M, Agostiano A, Cozzoli PD, Petrozza A, Lanzani G, Gigli G. Energy Environ Sci. 2013; 6:1565–1572.

10. Wang H, Kubo T, Nakazaki J, Segawa H. Phys Status Solidi RRL. 2014; 8:961–965.

11. Weidman MC, Beck ME, Hoffman RS, Prins F, Tisdale WA. ACS Nano. 2014; 8:6363–6371. [PubMed: 24840645]

12. Bae WK, Joo J, Padilha LA, Won J, Lee DC, Lin Q, Koh W, Luo H, Klimov VI, Pietryga JM. J Am Chem Soc. 2012; 134:20160–20168. [PubMed: 23131125]

13. Zhang J, Gao J, Church CP, Miller EM, Luther JM, Klimov VI, Beard MC. Nano Lett. 2014; 14:6010–6015. [PubMed: 25203870]

14. Zhang J, Gao J, Miller EM, Luther JM, Beard MC. ACS Nano. 2014; 8:614–622. [PubMed: 24341705]

15. Woo JY, Ko JH, Song JH, Kim K, Choi H, Kim YH, Lee DC, Jeong S. J Am Chem Soc. 2014; 136:8883–8886. [PubMed: 24919086]

16. Wang H, Kubo T, Nakazaki J, Kinoshita T, Segawa H. J Phys Chem Lett. 2013; 4:2455–2460.

17. Green MA, Emery K, Hishikawa Y, Warta W, Dunlop ED. Prog Photovoltaics. 2014; 22:701–710.

18. Shockley W, Queisser HJ. J Appl Phys. 1961; 32:510–519.

19. Guyot-Sionnest P. J Phys Chem Lett. 2012; 3:1169–1175. [PubMed: 26288053]

20. De Wolf S, Holovsky J, Moon SJ, Löper P, Niesen B, Ledinsky M, Haug FJ, Yum JH, Ballif C. J Phys Chem Lett. 2014; 5:1035–1039. [PubMed: 26270984]

21. Erslev PT, Chen H, Gao J, Beard MC, Frank AJ, van de Lagemaat J, Johnson JC, Luther JM. Phys Rev B. 2012; 86:155313.

22. Zhitomirsky D, Kramer IJ, Labelle AJ, Fischer A, Debnath R, Pan J, Bakr OM, Sargent EH. Nano Lett. 2012; 12:1007–1012. [PubMed: 22257205]

23. Zhao N, Osedach TP, Chang LY, Geyer SM, Wanger D, Binda MT, Arango AC, Bawendi MG, Bulovic V. ACS Nano. 2010; 4:3743–3752. [PubMed: 20590129]

24. Brown PR, Kim D, Lunt RR, Zhao N, Bawendi MG, Grossman JC, Bulovi V. ACS Nano. 2014; 8:5863–5872. [PubMed: 24824726]

25. Kemp KW, Labelle AJ, Thon SM, Ip AH, Kramer IJ, Hoogland S, Sargent EH. Adv Energy Mater. 2013; 3:917–922.

26. Nadenau V, Rau U, Jasenek A, Schock HW. J Appl Phys. 2000; 87:584–593.

27. Schmidt T, Lischka K, Zulehner W. Phys Rev B. 1992; 45:8989–8994.

28. Gao J, Zhang J, van de Lagemaat J, Johnson JC, Beard MC. ACS Nano. 2014; 8:12814–12825. [PubMed: 25485555]

29. Liu H, Tang J, Kramer IJ, Debnath R, Koleilat GI, Wang X, Fisher A, Li R, Brzozowski L, Levina L, Sargent EH. Adv Mater. 2011:3832–3837. [PubMed: 21766353]

30. Ehrler B, Musselman KP, Böhm ML, Morgenstern FSF, Vaynzof Y, Walker BJ, Macmanus-Driscoll JL, Greenham NC. ACS Nano. 2013; 7:4210–4220. [PubMed: 23531107]

31. Hoye RLZ, Ehrler B, Böhm ML, Muñoz-Rojas D, Altamimi RM, Alyamani AY, Vaynzof Y, Sadhanala A, Ercolano G, Greenham NC, Friend RH, MacManus-Driscoll JL, Musselman KP. Adv Energy Mater. 2014; 4:1301544. [PubMed: 26225131]

32. Franciosi A, Van de Walle CG. Surf Sci Rep. 1996; 25:1–140.

33. Brown PR, Lunt RR, Zhao N, Osedach TP, Wanger DD, Chang LY, Bawendi MG, Bulovi V. Nano Lett. 2011; 11:2955–2961. [PubMed: 21661734]

34. Gao J, Luther JM, Semonin OE, Ellingson RJ, Nozik AJ, Beard MC. Nano Lett. 2011; 11:1002–1008. [PubMed: 21291196]

35. Luther JM, Law M, Beard MC, Song Q, Reese MO, Ellingson RJ, Nozik AJ. Nano Lett. 2008; 8:3488–3492. [PubMed: 18729414]

36. Bozyigit D, Lin WMM, Yazdani N, Yarema O, Wood V. Nat Commun. 2015; 6:6180. [PubMed: 25625647]

37. Nagpal P, Klimov VI. Nat Commun. 2011; 2:486. [PubMed: 21952220]

38. Rath AK, Garcia de Arquer FP, Stavrinadis A, Lasanta T, Bernechea M, Diedenhofen SL, Konstantatos G. Adv Mater. 2014; 26:4741–4747. [PubMed: 24895324]

39. Oh SJ, Wang Z, Berry NE, Choi J, Zhao T, Gaulding EA, Paik T, Lai Y, Murray CB, Kagan CR. Nano Lett. 2014; 14:6210–6216. [PubMed: 25298154]

40. Bozyigit D, Wood V. J Mater Chem C. 2014; 2:3172–3184.

41. Yoon W, Boercker JE, Lumb MP, Placencia D, Foos EE, Tischler JG. Sci Rep. 2013; 3:2225. [PubMed: 23868514]

42. Zhitomirsky D, Voznyy O, Hoogland S, Sargent EH. ACS Nano. 2013; 7:5282–5290. [PubMed: 23701285]

43. Semonin OE, Luther JM, Choi S, Chen HY, Gao J, Nozik AJ, Beard MC. Science. 2011; 334:1530–1533. [PubMed: 22174246]

44. Talgorn E, Gao Y, Aerts M, Kunneman LT, Schins JM, Savenije TJ, van Huis MA, van der Zant HSJ, Houtepen AJ, Siebbeles LDA. Nat Nanotechnol. 2011; 6:733–739. [PubMed: 21946709]

45. Wanger DD, Correa RE, Dauler EA, Bawendi MG. Nano Lett. 2013; 13:5907–5912. [PubMed: 24256125]

46. Zhitomirsky D, Voznyy O, Levina L, Hoogland S, Kemp KW, Ip AH, Thon SM, Sargent EH. Nat Commun. 2014; 5:3803. [PubMed: 24801435]

47. Bozyigit D, Volk S, Yarema O, Wood V. Nano Lett. 2013; 13:5284–5288. [PubMed: 24164600]

48. Carey GH, Kramer IJ, Kanjanaboos P, Moreno-Bautista G, Voznyy O, Rollny L, Tang JA, Hoogland S, Sargent EH. ACS Nano. 2014; 8:11763–11769. [PubMed: 25376698]

49. Kim D, Kim DH, Lee JH, Grossman JC. Phys Rev Lett. 2013; 110:196802. [PubMed: 23705733]

50. Voznyy O, Zhitomirsky D, Stadler P, Ning Z, Hoogland S, Sargent EH. ACS Nano. 2012; 6:8448–8455. [PubMed: 22928602]

51. Jean J, Chang S, Brown PR, Cheng JJ, Rekemeyer PH, Bawendi MG, Grade ak S, Bulovi V. Adv Mater. 2013; 25:2790–2796. [PubMed: 23440957]

52. Kramer IJ, Zhitomirsky D, Bass JD, Rice PM, Topuria T, Krupp L, Thon SM, Ip AH, Debnath R, Kim HC, Sargent EH. Adv Mater. 2012; 24:2315–2319. [PubMed: 22467240]

53. Oh SJ, Berry NE, Choi JH, Gaulding EA, Paik T, Hong SH, Murray CB, Kagan CR. ACS Nano. 2013; 7:2413–2421. [PubMed: 23368728]

54. Dirin DN, Dreyfuss S, Bodnarchuk MI, Nedelcu G, Papagiorgis P, Itskos G, Kovalenko MV. J Am Chem Soc. 2014; 136:6550–6553. [PubMed: 24746226]

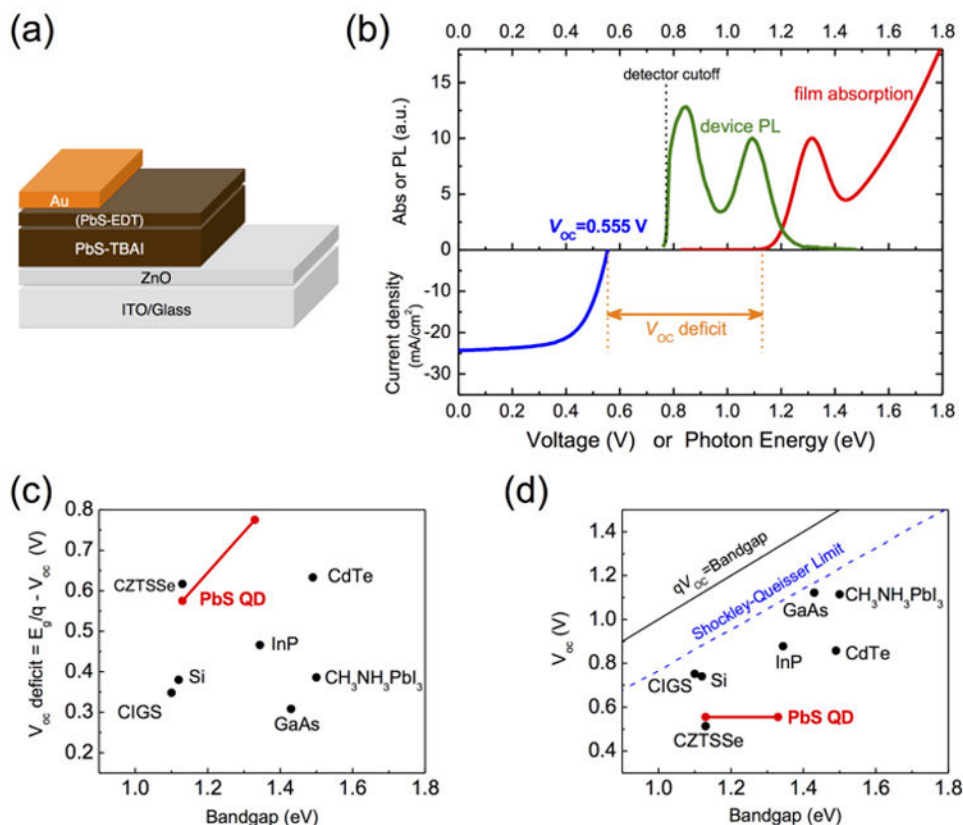55. Zhang H, Jang J, Liu W, Talapin DV. ACS Nano. 2014; 8:7359–7369. [PubMed: 24988140]

Figure 1.

V_{OC} deficit in PbS QDPV. (a) Device structure. The PbS-EDT QD layer is a thin electron-blocking layer between the PbS-TBAI QD absorber and Au electrode. ITO: indium tin oxide. (b) Upper panel: absorption spectra of a PbS-TBAI QD film and photoluminescence (PL) spectra of a PbS-TBAI QD/PbS-EDT QD device. Lower panel: J–V characteristics of the certified 8.6%-efficient QDPV (V_{OC} = 0.555 V).[8] (c) The V_{OC} deficits in PbS QDPV and other common PV materials. The two bandgap values shown for PbS QDs correspond to different definitions (see text). V_{OC} values correspond to certified record-efficiency devices.[17] CIGS: $CuIn_xGa_{1-x}Se_2$. CZTSSe: $Cu_2ZnSnS_xSe_{4-x}$. (d) Comparison of the V_{OC} and the absorber bandgap of various materials. The Shockley–Queisser limit at 300 K is also shown.
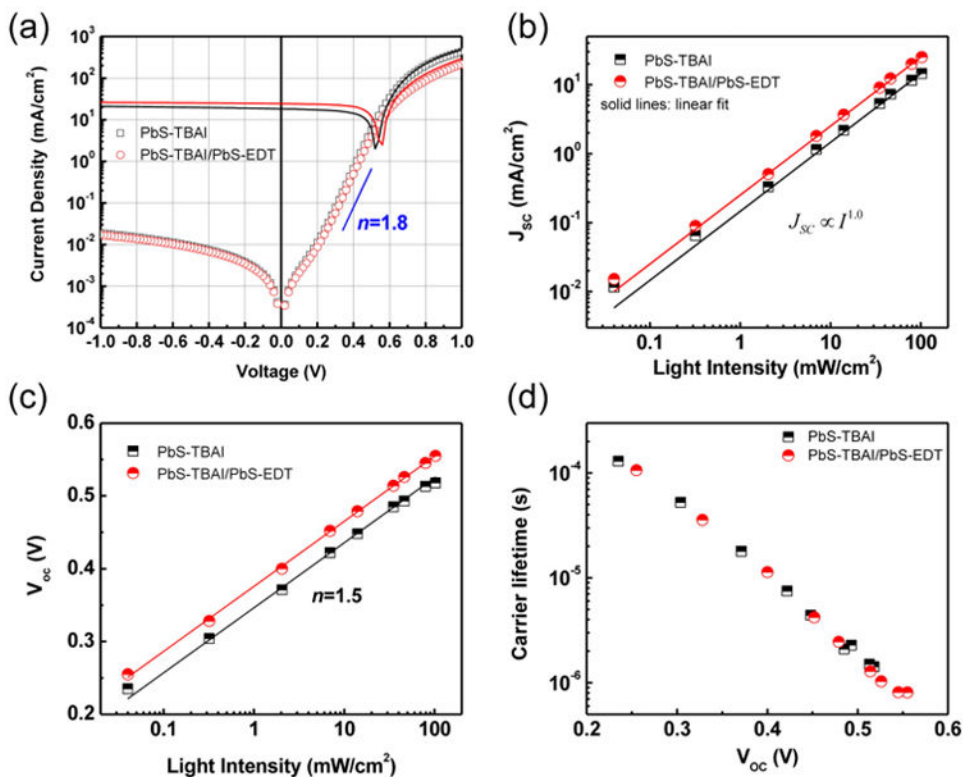
Figure 2.
Device characteristics of PbS-TBAI QD and PbS-TBAI QD/PbS-EDT QD devices. (a) *J–V* characteristics of devices in the dark (open markers) and under 100 mW/cm^2 AM1.5 illumination (solid lines). The straight line indicates the slope corresponding to an ideality factor $n = 1.8$. (b) Light-intensity dependence of J_{SC}. Solid lines: linear fits. (c) Light intensity dependence of V_{OC}. Solid lines: logarithmic fits with an ideality factor $n = 1.5$. (d) Carrier lifetime as a function of V_{OC}. Lifetimes are determined from transient photovoltage measurements with a varying steady-state white light bias to generate different V_{OC} values.
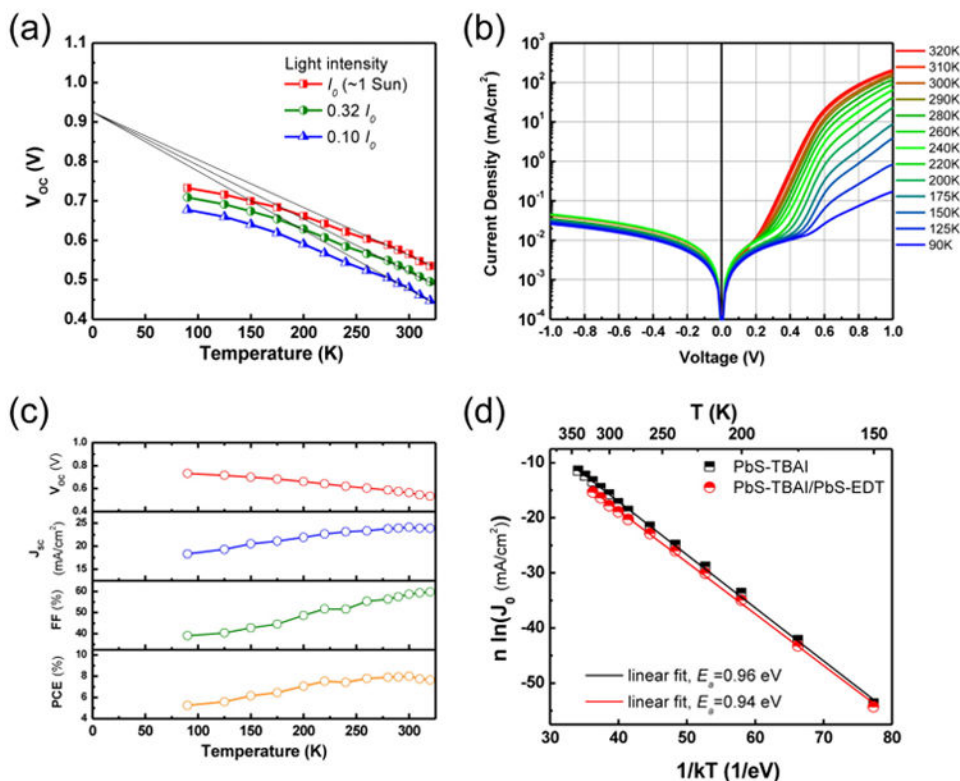
Figure 3.
Temperature dependence of PbS-TBAI QD/PbS-EDT QD QDPV performance. (a) Temperature dependence of V_{OC} under three different light intensities. Black lines: linear fits. (b) Temperature dependence of dark J–V characteristics. (c) Temperature dependence of photovoltaic parameters under ~1 sun illumination. (d) Relationship between $n \ln(J_0)$ and $1/kT$ (symbols) for estimation of the activation energy E_a. Values of n and J_0 are extracted by fitting the dark J–V curves shown in (b). Solid lines: linear fit corresponding to $E_a = 0.94 \pm 0.01$ eV for a PbS-TBAI QD/PbS-EDT QD device (red). The PbS-TBAI QD device shows similar behavior with an activation energy of 0.96 ± 0.01 eV (black).
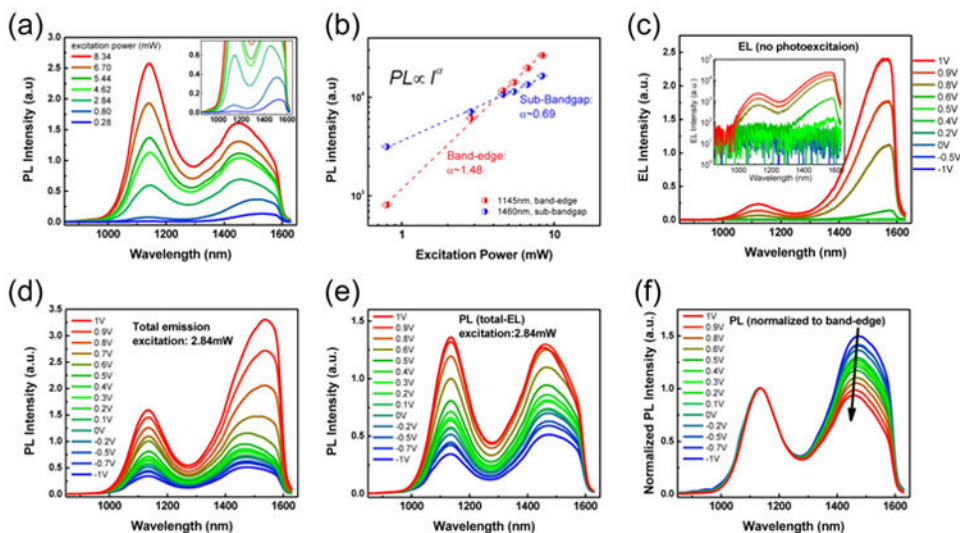
Figure 4.
Effect of sub-bandgap state-filling on the relative intensity of band-edge and sub-bandgap emission. Emission spectra are shown for a representative PbS-TBAI QD/PbS-EDT QD device. (a) PL spectra under different excitation powers (2.84 mW corresponds to an excitation intensity of ca. 120 mW/cm^2). Inset: magnified spectra at low excitation intensities. At low intensities, the sub-bandgap emission blue-shifts with increasing excitation power. (b) Excitation power dependence of the PL intensity for the band-edge emission (∼1145 nm) and the sub-bandgap emission (∼1460 nm) peaks. Dotted line: power law fits. (c) EL spectra with varying applied biases. Inset: semilog plot. The EL turn-on voltage is ∼0.5 V, and no EL signal is detected under reverse bias. (d) Total (PL+EL) emission spectra under 2.84 mW photoexcitation with varying applied biases. The emission spectra include the contribution from both PL and EL. (e) PL contribution to total emission shown in (d). PL spectra are calculated by subtracting EL spectra from the total emission. We note that the PL signal is only from the excitation spot (∼2.4 mm^2), whereas the EL signal is from the entire device (5.44 mm^2). (f) Normalized PL spectra under varying applied bias. The spectra are normalized to the peak band-edge emission. With increasing applied bias, the ratio of sub-bandgap PL to band-edge PL decreases and the sub-bandgap PL blue-shifts slightly, likely due to sub-bandgap state filling by injected carriers.
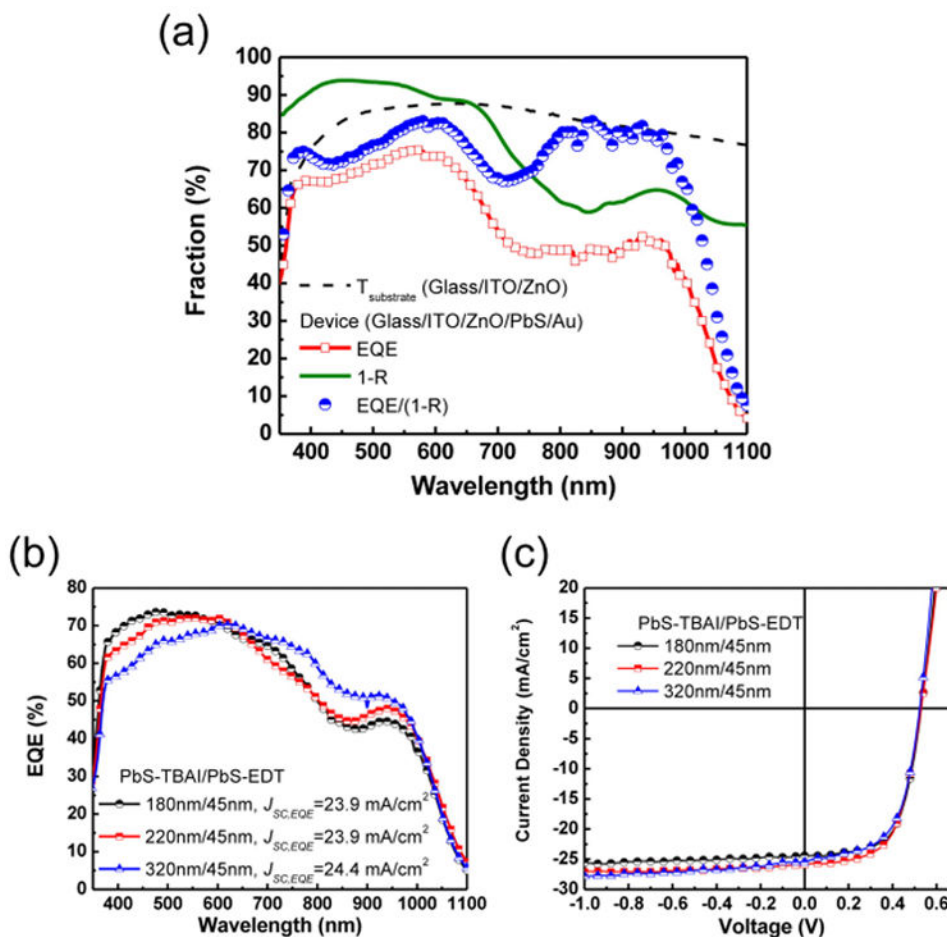
Figure 5.
Inefficient photocurrent collection efficiency of thicker PbS-TBAI QD/PbS-EDT QD solar cells. (a) The EQE, $1 - R$, and EQE/$(1 - R)$ spectra of a thin PbS-TBAI QD(220 nm)/PbS-EDT QD(45 nm) device; R is the diffuse reflectance of the device. The $1 - R$ represents an upper bound for PbS QD absorption so EQE/$(1-R)$ represents a lower bound for IQE in the PbS QD layer. The transmittance of the substrate (glass/ITO/ZnO) $T_{substrate}$ is also shown. The device shows lower EQE at long wavelengths due to insufficient photon absorption. (b) EQE spectra of PbS-TBAI QD/PbS-EDT QD devices with different PbS-TBAI QD absorber thicknesses. Expected short-circuit current densities ($J_{SC,EQE}$) are calculated by integrating the EQE with the AM1.5 solar spectra (100 mW/cm^2). Thicker devices benefit from increased absorption of long-wavelength photons at the expense of carrier collection efficiency. (c) J–V characteristics of the devices shown in (b).